communications earth & environment

ARTICLE

https://doi.org/10.1038/s43247-023-01035-6 OPEN

The westerly winds control the zonal migration of rainy season over the Tibetan Plateau

Xingwen Jiang [1✉], Fenying Cai[2], Zhenning Li [3], Zunya Wang[4] & Tuantuan Zhang[5,6]

Precipitation over the Tibetan Plateau is modulated by both the South Asian summer monsoon and the mid-latitude westerly winds. Using observations and numerical simulations, this study highlights the out-of-phase relationships between the mid-latitude westerly wind speeds and the west-east migration of Tibetan Plateau rainy season. When the westerly jet shifts northward before July, the weakening of westerly winds over the Tibetan Plateau leads to a westward shift of low-level warm air center and a westward extension of moist air convergence. Consequently, rainy season advances westward. Conversely, the southward shift of westerly jet after August leads to a strengthening of westerly winds and an eastward retreat of rainy season. Numerical simulations confirm the dominant role of mid-latitude westerly winds on the rain belt migration over the Tibetan Plateau, and further indicate that the timing of the westward extension of rain belt is determined by the weakening of mid-latitude westerly winds.

[1] Heavy Rain and Drought-Flood Disasters in Plateau and Basin Key Laboratory of Sichuan Province, Institute of Tibetan Plateau Meteorology, China Meteorological Administration, Chengdu, Sichuan 610072, China. [2] Potsdam Institute for Climate Impact Research (PIK), Member of the Leibniz Association, Potsdam 14473, Germany. [3] Division of Environment and Sustainability, The Hong Kong University of Science and Technology, Hong Kong, China. [4] National Climate Center, China Meteorological Administration, Beijing 100081, China. [5] School of Atmospheric Sciences, Sun Yat-sen University, Southern Marine Science and Engineering Guangdong Laboratory (Zhuhai), Zhuhai, Guangdong 519082, China. [6] Guangdong Province Key Laboratory for Climate Change and Natural Disaster Studies, Sun Yat-sen University, Zhuhai, Guangdong 519082, China. ✉email: xingwen.jiang@yahoo.com

The Tibetan Plateau (TP), also known as the 'Asian water tower', is the source of several major Asian rivers, including the Yellow River, Yangtze River, Brahmaputra River, Mekong River, and the Indus River, providing a huge amount of freshwater for ecosystems and billions of people in Asia[1]. Variations of precipitation type (e.g., rainfall and snow) and amount affect not only the water cycle but also energy cycle over the TP, and thereby exert a great impact on regional and even global weather and climate due to elevated heating over the TP by an average altitude above 4000 m[2,3]. The precipitation over the TP varies on multiple timescales and is modulated by tropical monsoons and mid-latitude westerly winds, which affect the moisture budget over the TP[4]. The precipitation over the TP also exhibits remarkable spatiotemporal heterogeneity due to the complex topographic and geographic conditions[4–6]. In general, summertime precipitation over the TP decreases from south and east to north and west[4]. Based on the annual cycle of stable oxygen isotope ratio in precipitation, Yao et al. (2013) suggested that moisture over the southern TP and the northern TP are mainly controlled by the South Asian summer monsoon (SASM) and the mid-latitude westerly winds[7], respectively; and the transition in between (mostly 30°–35°N) was dominated by interaction between the SASM and the westerly winds. The precipitation anomalies over the TP are linked to anomalies of moisture input through its southern boundary associated with the anomalies of the SASM[8–10]. Although the mid-latitude westerly winds and the SASM are recognized as key atmospheric systems that influence precipitation over the TP, their related physical processes and impact mechanisms are mostly limited to the influence of water vapor transport.

The climate over the TP is characterized by distinct dry and rainy seasons. Most TP receives nearly 80% of annual accumulated precipitation from May to September (Supplementary Fig. S1). In general, the rainy season on the TP begins in the east and southeast around early May and progresses gradually westward, with the western TP experiencing the rainy season by early July at the latest[11,12]. The rainy season retreats in reverse, starting from the western TP around late August and ending in the eastern TP around early October. Therefore, the duration of the rainy season on the TP gradually shortens from east to west, and the precipitation decreases accordingly. Both the onset and retreat dates of rainy season exhibit strong variability on both interannual and interdecadal timescales. In the recent six decades, the duration of rainy season has lengthened significantly as the rainy season starts earlier and ends later[13]. The earlier onset leads to the increased rainfall in May in the southeastern and central TP, contributing to local lake expanding and greening in recent decades[14,15]. In addition, the variation of rainy season onset and retreat in the southern TP was suggested to be linked to the variation of the SASM on interannual timescale[12]. Then, how do the mid-latitude westerly winds affect the rainy season on the TP? In this analysis, the influence of the mid-latitude westerly on the zonal migration of the rainy season is investigated from the perspective of climatology.

The annual cycle of the westerly winds greatly affects the weather and climate inside and outside the TP. During winter, the westerly jet stream is located south of the TP, while in summer, it moves north of the TP[16]. The westerly winds migrate from south of the TP in the spring to north of the TP in the midsummer, partly driven by dynamic and thermodynamic forcings of the TP[2]. The interaction of westerly winds with the TP significantly influences the Asian summer monsoon by several ways[17–19]. As airs over the TP are warmer and wetter than those in the middle troposphere of the nearby regions[20], changes in position and magnitude of the westerly winds significantly modulate horizontal advection of temperature and moisture downstream and thereby vertical motions over East Asia[21]. In the meantime, the annual cycle of westerly winds also affects spatial patterns of moisture and temperature, as well as synoptic disturbances over the TP[22]. Despite these studies, the possible role of the westerly winds in the seasonality of precipitation over the TP remains unexplored.

The purpose of the study is to investigate the possible impacts of the annual cycle of the mid-latitude westerly winds on the precipitation over the TP from the perspective of climatology. First, observational results demonstrate that the west-east migration of rainy season onset is linked to the north-south migration of the westerly winds by analyzing wind convergence and moisture convergence. Then, numerical simulations are conducted to confirm the results in observations and investigate the different contributions of the tropical atmospheric circulation and the westerly winds to the onset and retreat of rainy season in the TP.

Results

Observation. The precipitation in the TP and adjacent areas generally decreases from low latitudes to high latitudes from May to October, and the precipitation on the TP is less than that to south and east of the TP (Fig. 1). Areas with relatively high precipitation (more than 2 mm day^{-1} for example) extend westward along South Asia and the southern TP from May to July (Fig. 1a–c, 2a), and retreat eastward from August to October (Figs. 1d–f, 2a). These features are also seen from other thresholds of precipitation rate and data sources (Figs. S2 and S3). Such a west-east migration features the rainy season on the TP. The northwestward development of the SASM leads to increase of the summertime precipitation in southwestern slopes of the TP and the formation of the summer maximum precipitation center in the western TP (Fig. 2a), while the wintertime precipitation in the western and southwestern slopes of the TP is mainly caused by the orographic lift of westerly winds. The low-level winds over the TP weaken in summer, while the monsoon circulation in the tropics strengthens (Figs. 1, 2b, and Supplementary Fig. S4). In particular, the 600-hPa winds generally show a convergent pattern during May to October, with northwesterly winds and southwesterly winds over the northern and southern TP, respectively (Fig. 1); but these features manifest substantial variations of westerly wind speed. In the upper troposphere, the westerly jet stream exhibits a north-south migration during May to October (Supplementary Fig. S4). It is located to the south of TP before March, starts to migrate northward in April, and reaches the northeast position in July (Supplementary Fig. S4a–g). The southward migration of the westerly jet occurs in August, and returns to the south of TP in October (Supplementary Fig. S4h–j). As such, the TP experiences the lowest westerly wind speed in both 200-hPa and 600-hPa levels in July and August (Fig. 2). On the other hand, southerly winds over the southern TP (28°–30°N, Fig. 1) are weak and only exhibits weak seasonal cycle (Fig. 2c–d). In general, the SASM exhibits a west-east migration[23] but a north-south migration is observed for the mid-latitude westerly winds. The migration direction of rainy season in the TP is similar to the SASM but difference from the westerly winds. What are the possible roles of the westerly winds play in the zonal migration of the rainy season on the TP?

To investigate the possible effects of the mid-latitude westerly winds on the rainy season on the TP, the moisture convergence, which provides the necessary moisture source for precipitation over the TP is analyzed. Moist airs basically converge over the east but diverge over the west (Fig. 3a). The maximum of moisture convergence is basically located near the 95°E all year around (Fig. 3a, b and Supplementary Fig. S5), while precipitation

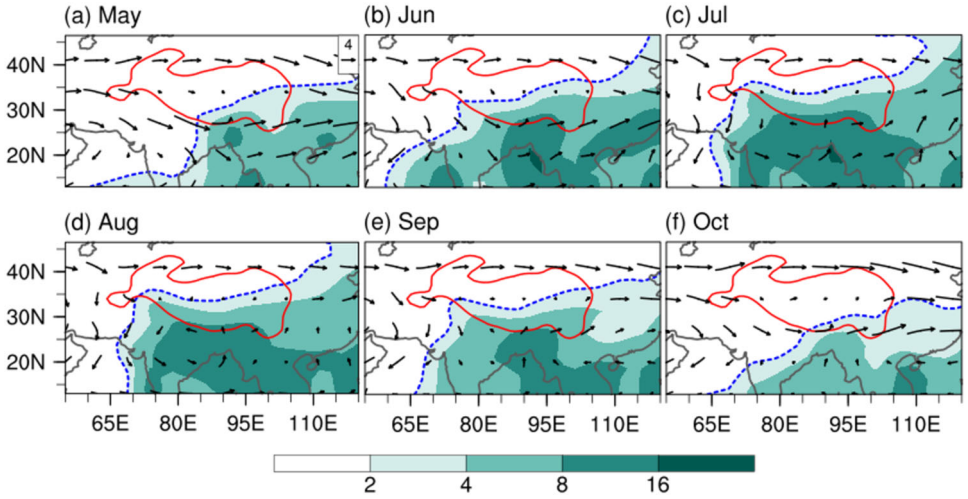

Fig. 1 Climatological monthly rainfall and atmospheric circulations at 600 hPa. The shadings indicate GPCP precipitation (units: mm day^{-1}) and vectors represent ERA5 atmospheric circulations at 600 hPa (units: m s^{-1}) in **a** May, **b** June, **c** July, **d** August, **e** September and **f** October. Red solid contours denote the terrain height of 2000 m. Blue dashed contours are 2 mm day^{-1} isolines of rainfall.

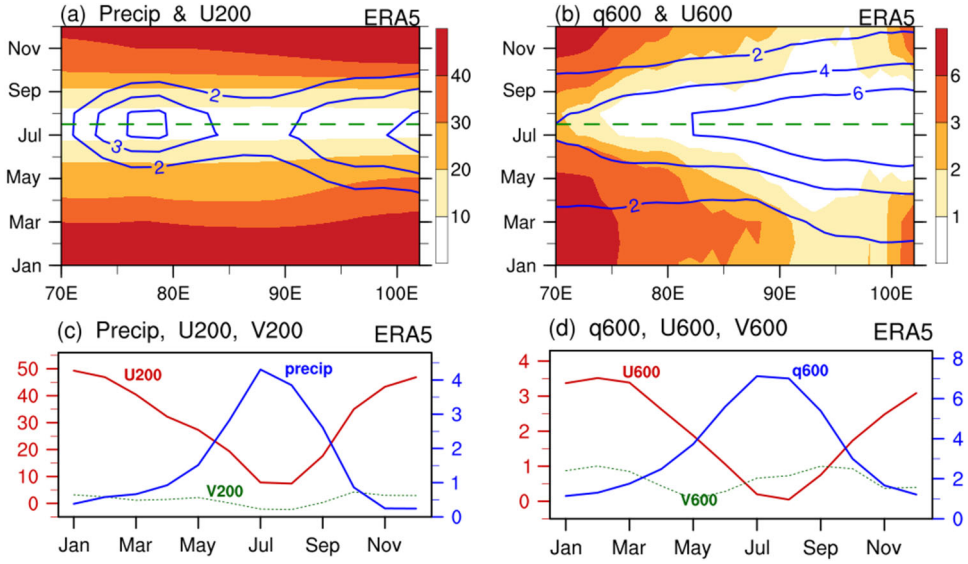

Fig. 2 Climatological annual cycle of zonal wind, rainfall, and specific humidity. a Zonal wind at 200 hPa (shadings; units: m s^{-1}), precipitation (contours; units: mm day^{-1}), and **b** zonal wind at 600 hPa (shadings; units: m s^{-1}) and specific humidity at 600 hPa (shadings; units: g kg^{-1}) averaged over 28°–35°N. **c** zonal wind at 200 hPa (red solid; units: m s^{-1}), precipitation (blue solid; units: mm day^{-1}), and **d** zonal wind at 600 hPa (red solid; units: m s^{-1}), and specific humidity at 600 hPa (blue solid; units: g kg^{-1}) averaged over 28°–35°N, 75–105°E. Meridional wind at 200 hPa and 600 hPa (green dashed; units: m s^{-1}) averaged over 28°–30°N, 75–105°E are also plotted in **c** and **d**, respectively. The precipitation is from GPCP dataset, while other variables are from ERA5 reanalysis dataset.

decreases from the east to the west (Fig. 1). This inconsistency may partly be ascribed to deficiencies in either reanalysis or precipitation data. As shown in Fig. S6, the maximum precipitation is ascribed to the high moist over the Brahmaputra Grand Canyon. Despite this inconsistence, the western boundary of moisture convergence zone migrates from the east to the west from January to August, and then retreats eastward (Fig. 3b), consistent with the seasonal variation of western boundary of the main precipitation zone (Figs. 1, 2a).

The pattern of the moisture divergence zone at 600 hPa is highly similar to that at other low levels over the TP. To reveal the relative contribution of moisture and winds to this evolution of moisture divergence, we analyze seasonal variation of moisture and divergence at 600-hPa level. The 600-hPa moisture generally decreases from the east to the west, while the maximum appears over the central-eastern TP in July and August (Supplementary Fig. S6). Wind generally diverges over the west but converges over the east (Fig. 3a). The western boundary of the wind convergence moves westward from January to July and then moves eastward after August. The maximum wind convergence is located around 92°E all year round and peaks in June (Fig. 3a). The comparison of wind divergence, moisture, and water vapor flux divergence indicates that the variation of the western boundary of the water vapor convergence zone and the longitudinal position of the moisture convergence center are closely related to variations of both wind divergence and moisture (Figs. 2b, 3a, b).

Why does the western boundary of the moisture convergence zone migrate westward? As shown in Fig. 3a, c, and Supplementary Fig. S6, the wind convergence at the eastern TP is accompanied by local low pressure. The center and western

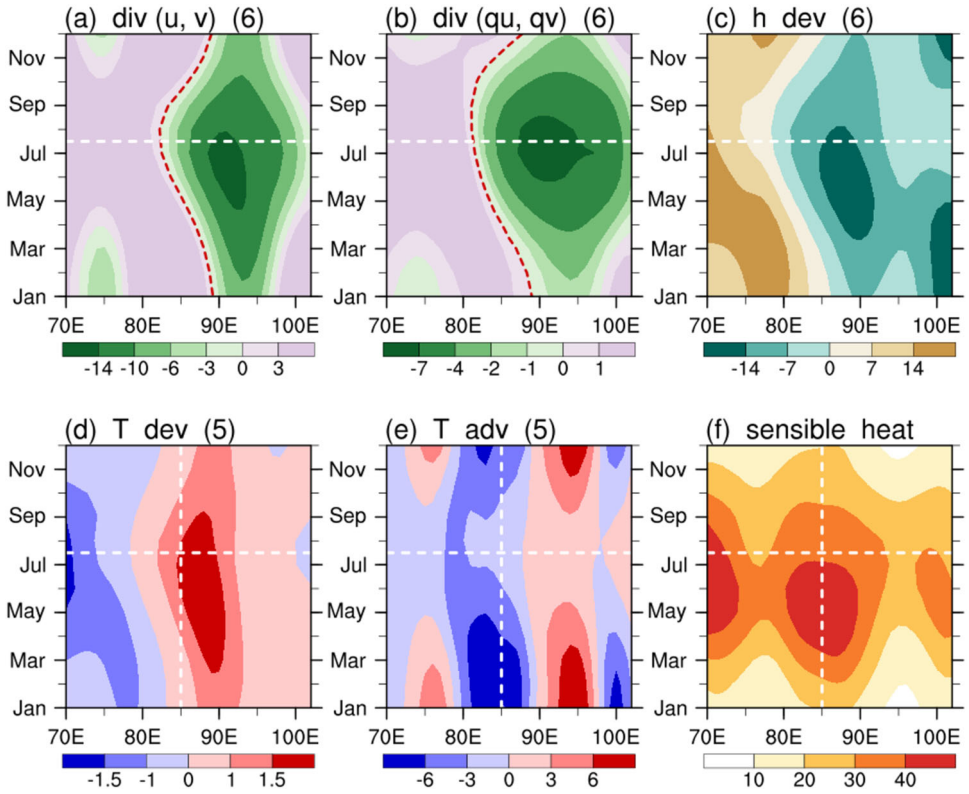

Fig. 3 Climatological annual cycle of divergence, moisture flux divergence, geopotential height, atmospheric temperature, temperature advection, and sensible heat flux. a Divergence (units: $10^{-7}\,s^{-1}$) at 600 hPa, **b** divergence of moisture flux (units: $10^{-6}\,g\,kg^{-1}\,s^{-1}$) at 600 hPa, **c** geopotential height deviation (units: gpm) at 600 hPa, **d** temperature deviation (units: K) at 500 hPa, **e** temperature advection ($-u\frac{\partial T}{\partial x}$; units: 10^{-6} K s^{-1}) at 500 hPa, and **f** surface upward sensible heat flux (units: 10^5 J m^{-2}). The values in a–f are averaged from 28°–35°N. The values in **c**, **d** are deviations from the zonal mean over 65°–105°E. Convergence and divergence near 85°E are separated by red dashed lines (div = 0) in **a**, **b**. White horizonal and vertical dashed lines in **a**–**f** denote when time is late-July and where longitude is 85°E, respectively.

boundary of the low-pressure zone show a similar seasonal migration to wind divergence. The low-pressure areas are basically overlapped with the warmer air areas (Fig. 3c, d, and Supplementary Fig. S6, S7). The air temperature at low levels is directly affected by surface heating via atmospheric boundary turbulence (Fig. 3d, f). Due to elevated surface heating, the 500-hPa air temperature over the TP is higher than that at the same elevation over the nearby areas, with the center located at 85°–90°E. As westerly winds prevail over the TP, zonal cold and warm advection are located to the west and east of the maximum temperature center, respectively (Fig. 3d, e, and supplementary Fig. S7). Thus, the center of maximum surface heating is expected to be located to the west of the temperature center (Fig. 3d, f, and Supplementary Fig. S7, S8). Indeed, as shown in supplementary Fig. S8, the maximum surface sensible flux is mostly located at southern-central TP (75°–90°E), where the dry land is covered by little vegetation. By contrast, the sensitive heat flux is lower on the western TP due to high albedo caused by snow and ice cover, and is also lower on the eastern TP with high vegetation cover. During the period from April to July, the zonal wind speed decreases, leading to a weakening of the zonal horizontal advection of temperature (as shown in Fig. 3e and Supplementary Fig. S7). Consequently, the maximum temperature center moves westward close to the center of maximum surface sensible flux (Fig. 3d, f, and Supplementary Fig. S7, S8). Additionally, the 600-hPa moisture is higher than that at the same elevation due to the direct supplement of moisture by surface evaporation. Thus, the weakening of westerly winds reduces the input of dry air at the western TP and the output of moisture air at the eastern TP. Therefore, moisture accumulates and peaks over the central TP in July, when the westerly winds reach the weakest status. The reverse processes occur with an increase in westerly wind speed from August to October.

The above analyses indicate that the annual cycle of westerly winds pronouncedly affects the spatiotemporal variation of moisture, temperature, pressure, and winds over the TP at the lower levels, and thereby, the variation of precipitation. As shown in Fig. 2, the zonal variation of 600-hPa moisture is out-of-phase with that of westerly wind speed. The gradual increase in precipitation during summertime is accompanied by an increase in moisture but a decrease in zonal wind speed from low levels to high levels. It is important to note that the increase in moisture over the TP is not necessarily accompanied by an increase in southerlies over the southern TP, as the moisture at the lower levels over the TP is higher than that at the same altitude over the nearby areas. Overall, the west-east migration of rainfall, the moisture flux convergence, the 600-hPa low pressure, the 500-hPa warm temperature, and the sensible heating center are closely linked to the annual cycle of westerly wind speed over the TP.

Simulations. To verify the impact of the mid-latitude westerly winds on the zonal migration of the rainy season on the TP, numerical simulations are conducted using the Community Earth System Model (CESM).

As shown in supplementary Fig. S9, the numerical simulation well captured the spatial-temporal variation of precipitation over the TP when the circulation outside of the TP is nudging to the status of the observation (refer to as the experiment NG). The main precipitation domain extends westward in the southern TP

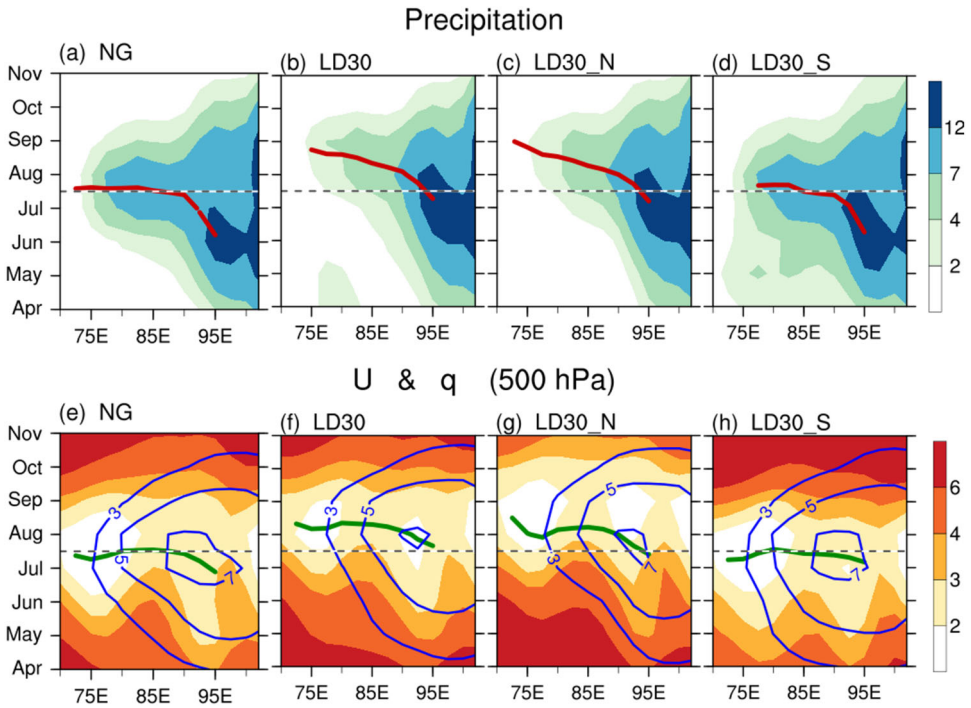

Fig. 4 Simulated evolution of precipitation, zonal wind, and moisture. a–d Precipitation (units: mm day^{-1}), and **e–h** zonal wind at 500 hPa (shadings; units: m s^{-1}) and specific humidity at 500 hPa (contours; units: g kg^{-1}) averaged over 28°–35°N. (**a**, **e**), (**b**, **f**), (**c**, **g**), (**d**, **h**) show the results of experiment NG, LD30, LD30_N, LD30_S, respectively. Red lines in **a–d** (green lines in **e–h**) denote the date when rainfall (moisture) reach its maximum on different longitudes. Gray dashed lines in **a–h** denotes when time is late-July.

from May to July (Fig. 4a, Supplementary Fig. S9a–c), and then retreats eastward from August to October (Fig. 4a, and Supplementary Fig. S9d–f), indicating an apparent west-east migration of western boundary of main precipitation domain in the model simulation. Moreover, the westward extension and eastward retreat of main precipitation domain are accompanied by apparent weakening and strengthening of westerly winds, respectively. The similarity of the results of experiment NG and observations confirms the model is suitable to conduct subsequent simulation experiments.

When the 30-day-lagged climatological winds and temperature are imposed on corresponding variables outside of the TP during integration (the experiment LD30), the rainy season on the TP still exhibits the obvious east-west migration. However, the simulated annual cycle of the circulations in both mid-latitudes and tropics lags by one month in the NG compared to that in the LD30 (Fig. 4e, f, and supplementary Fig. S10). Correspondingly, the zonal migration of the rainy season on the TP delays by one month. It is observed that the peak of precipitation in the central and western TP occurs in middle July in the NG but during middle August in the LD30 (Fig. 4a, b, and Supplementary Figs. S10, S11). Evidently, the nudging method is proved to be reasonable to study the impact of circulations outside of the TP on the rainy season on the TP. Moreover, this experiment indicated that the combination of mid-latitude westerly winds and tropical atmospheric systems (e.g., the South Asian summer monsoon) outside of the TP determines the occurrence and zonal migration of rainy season on the TP.

Why is the annual cycle of precipitation over the TP lagged? As shown in Fig. 4e, f, the annual cycle of westerly wind speed is lagged in the simulations, so do the moisture and temperature (Figs. 4e, f, 5e, f). The maximum precipitation is basically accompanied by the weakest westerly winds and the maximum moisture in the simulations (Fig. 4a, b, e, f). Before August, the delayed decrease in westerly wind speed leads to a delayed weakening of the zonal cold advection on the west of the warm center (Fig. 5a, b). Consequently, the lagged westward extensions of the warm air and low-pressure centers result in the delayed westward extension of rainy season (Figs. 4a, b, 5a, b, e, f, and supplementary Fig. S10). Reverse processes are also noticed as westerly wind speed increases after August, consistent with those in observations.

To emphasize the influence of mid-latitude westerly winds on the zonal migration of the rainy season on the TP, two additional experiments are conducted: the LD30_N and LD30_S. In the LD30_N experiment, only the atmospheric circulation to the north of 27°N is lagged, and the spatial-temporal evolution of precipitation on the TP is delayed by one month, similar to the output of the LD30 experiment (as shown in Fig. 4c, g, and Supplementary Figs. S10–S12). Conversely, in the LD30_S experiment, only the atmospheric circulation to the south of 27°N is lagged, and the rainy season on the TP and its zonal migration occur at normal times, consistent with the results of the NG experiment (as illustrated in Fig. 4d, h, and Supplementary Figs. S10–S12). This compassion indicates that the annual cycle of precipitation over the TP is dominated by the atmospheric circulation to the north of the 27°N, where westerly winds prevail. Moreover, the connections of the precipitation with the westerly winds, moisture, and air temperature in all the simulations resemble those in the observation, confirming the important role of the mid-latitude westerly winds.

Conclusions

The TP is characterized by distinct dry winter and wet summer. It is well accepted that the summer precipitation over the TP is affected by both the SASM and the westerly winds. However, their dissimilar impacts on the seasonal cycle of precipitation over the TP are not well explored. Geographically, precipitation in the southern TP is more likely affected by the SASM to its south, while the northern TP precipitation is more susceptible to the westerly

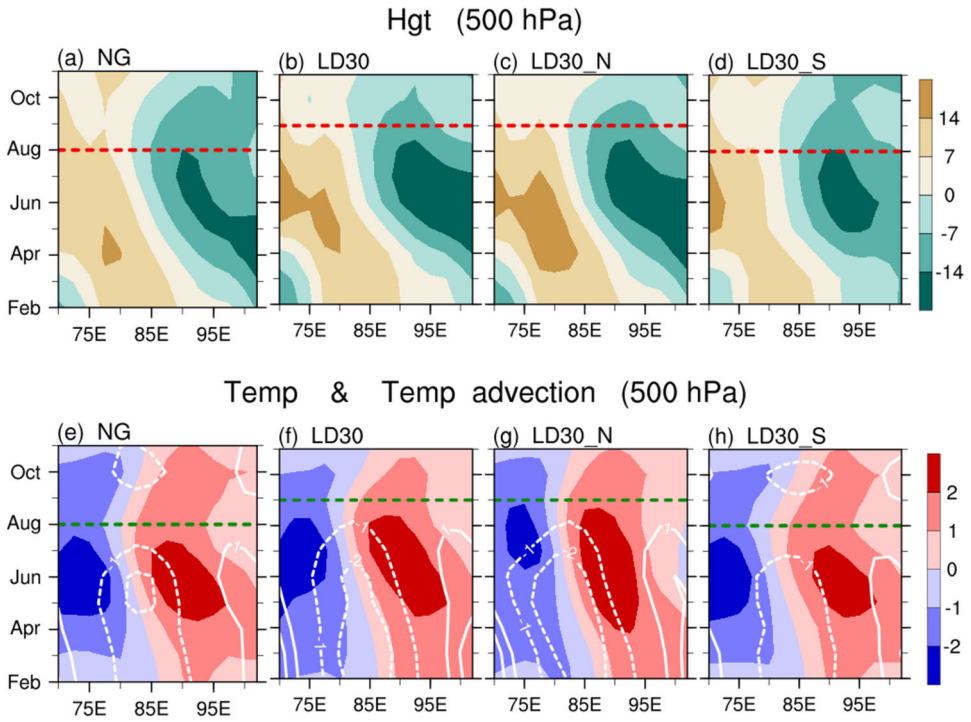

Fig. 5 Simulated evolution of geopotential height, atmospheric temperature, and temperature advection. The evolution of **a**–**d** geopotential height deviations at 500 hPa (shadings; units: gpm) and **e**–**h** atmospheric temperature deviations (shadings; units: K), zonal temperature advection (contours; units: 10^{-6} K s^{-1}) at 500 hPa averaged over 28°–35°N. The values in **a**–**h** are deviations from the zonal mean over 65°–105°E. (**a**, **e**), (**b**, **f**), (**c**, **g**), and (**d**, **h**) show the results of experiment NG, LD30, LD30_N, and LD30_S, respectively. Colorful horizontal dashed thick lines in **a**, **d**, **e**, **h** (in **b**, **c**, **f**, **g**) denote when time is August (September).

winds aloft, as the westerly jet is located around the northern boundary of the TP. While the air transported by the SASM is warm and moist, the air transported by the westerly is cold and dry, resulting in higher summertime precipitation amount over the southern TP compared to the northern TP. In this study, however, we found the rainy season in terms of timing and duration over the TP exhibits an apparent zonal asymmetry. The advance and retreat of rainy season over the TP present a west-east migration pattern, which is mostly controlled by the annual cycle of the westerly. The annual cycle of precipitation is out-of-phase with that of westerly wind speed over the TP. The weakening of westerly winds favors more precipitation over the TP by reducing input of dry and cold air at the west and output of moist and warm air at the east. The elevated surface heating center in the western TP induces a low-level warm air center and a low-pressure center, whose position relative to the surface heating center depends on the westerly speed. The weakening of westerly winds over the TP before July, as a result of the northward shift of westerly jet, leads to westward shifts of the warm air center and the low-pressure center, as well as westward extension of moist air. Consequently, the rainy season advances westward. After August, the southward shift of westerly jet leads to a strengthening of westerly winds and an eastward retreat of rainy season. In contrast, the results of sensitivity experiments indicate that the west-east migration of the TP rainfall does not change notably when the SASM is delayed for one month. Thus, this study suggests that the onset and retreat of rainy season over the TP is mostly controlled by the seasonal cycle of mid-latitude westerly winds.

Precipitation over the TP exhibits variations on a wide range of timescales, and the origins varies for various time scales. While the intra-seasonal and interannual variability of summertime precipitation is linked to interactions of the SASM anomalies and wave-like atmospheric circulation anomalies over mid-latitude[9,10], the inter-decadal variability of the summertime precipitation over the TP was suggested to be linked to the westerly (Fig. S5)[24,25,26]. This study investigates the annual cycles of precipitation over the TP and mid-latitude westerly winds, suggesting that summer weakening of westerly winds favors more precipitation over the TP and westward extension of main precipitation zone in the south-eastern TP. In addition, Wang et al. (2022) indicated that increased westerly winds led to late onset of rainy season over the TP[13]. Given the strong link between westerly winds and precipitation over the TP, it is recommended to consider the response of westerly winds to global warming for summertime precipitation projection. Furthermore, the possible feedback of the SASM heating on the westerly winds warrants further studies.

Methods

Data. Monthly mean precipitation data from the Global Precipitation Climatology Project[27] (GPCP, with a resolution of 2.5° × 2.5°) and Climatic Research Unit (CRU dataset[28] with a resolution of 0.5° × 0.5°), and the ERA5 monthly data[29] on single level and pressure levels from 1000 hPa to 100 hPa (with a resolution of 1.0° × 1.0° interpolated from 0.25° × 0.25°) are adopted in this study. The monthly data from 1981 to 2010 are averaged into 30-year long-term mean before further analysis.

Model and simulations. The atmospheric component of the Community Earth System Model (CESM) Version 1.2.2, the Community Atmospheric Model (CAM) Version 5[30] is used to investigate the role of the westerly in modulating the rainy season migration in the TP. We implement the "F_2000_CAM5PM" component setting for the model, in which the solar forcing, carbon dioxide, ozone concentration, and aerosol loadings, are all fixed at the levels of year 2000. The atmospheric resolution in the CESM CAM5 is 1.9° × 2.5° in longitude-latitude with 30 vertical levels.

Table 1 Experiment design.

Experiment names	Design
NG	Nudging toward ERA-5 daily climatology (0-day lag time) over the globe except for the TP region (60°E–105°E/27°N–40°N)
LD30	Nudging toward ERA-5 daily climatology with a 30-day lag time (e.g., nudge the 1st Julian Day ERA-5 climatology into the model state on the 31st model Julian Day) over the globe except for the TP region (60°E–105°E/27°N–40°N)
LD30_N	Nudging toward ERA-5 daily climatology with a 30-day lag time over the region where the latitude is north to 27°N, and with 0-day lag time south to 27°N, except for the TP region (60°E–105°E/27°N–40°N)
LD30_S	Nudging toward ERA-5 daily climatology with a 30-day lag time over the region where the latitude is south to 27°N, and with 0-day lag time north to 27°N, except for the TP region (60°E–105°E/27°N–40°N)

The nudging (Newton relaxation) technique is implemented through all model layers to impose an ERA-5 based daily climatology (including zonal wind, meridional wind, and temperature) into the model integration. Specifically, the zonal wind prognostic equation with a nudging term can be written as

$$\Delta \mathrm{U} = \sum\left(\frac{\partial u}{\partial t}\right)_i \Delta t + (G\Delta t)\cdot(U_{ana} - U_{mod}) \quad (1)$$

Where ΔU is the updating zonal wind change, consisting of all physical forcing terms $\sum(\frac{\partial u}{\partial t})_i \Delta t$ and a nudging (non-physical) forcing term $(G\Delta t)\cdot(U_{ana} - U_{mod})$. In the nudging term, G is a constant, known as the specified relaxation parameter; U_{ana} is the value of the nudged zonal wind in the prescribed analysis field; U_{mod} is the zonal wind variable in the model. Δt represents the dynamical time-step size. The tricky point is to determine a relaxation parameter to ensure that the nudging term is effective but does not dominate the prognostic equation. By multiple tests, $G = 1/5$ (day^{-1}) is suitable to both produce an ERA-5-like daily climatology and maintain the reasonable day-to-day synoptic disturbances.

We designed four groups of experiment to reveal the contribution of the westerly winds and tropical atmospheric circulation to rainy season migration in the TP (see Table 1). To mimic the lagged westerly migration over certain zonal belts, a 30-day lag time (e.g., nudge the 1st Julian Day ERA-5 climatology into the model state on the 31st model Julian Day) is implemented in LD30, LD30_N, and LD30_S. In all experiments, no nudging term is imposed on the TP region (60°E–105°E/27°N–40°N). In other word, pure responses to the peripheral westerly migration over the TP region could be obtained. All model experiments are integrated for 35 years. The first 5-year integration is regarded for spin-up of the land surface model, and the outputs from year 6 to year 35 (30 years) are used for investigating the model responses.

Data availability

The GPCP and CRU datasets are available online (https://psl.noaa.gov/data/gridded/data.gpcp.html and https://crudata.uea.ac.uk/cru/data/hrg/). The ERA5 dataset could be download freely from https://doi.org/10.24381/cds.6860a573.

Code availability

All figures in this study are created by NCAR Command Language. The codes used to generate the results of this study are available on request from the authors.

Received: 23 March 2023; Accepted: 29 September 2023;
Published online: 09 October 2023

References

1. Immerzeel, W., Beek, L. & Bierkens, M. Climate change will affect the Asian Water Towers. *Science* **328**, 1382–1385 (2010).
2. Wu, G. et al. Tibetan Plateau climate dynamics: recent research progress and outlook. *Natl Sci. Rev.* **2**, 100–116 (2015).
3. Liu, Y. et al. Land–atmosphere–ocean coupling associated with the Tibetan Plateau and its climate impacts. *Natl Sci. Rev.* **7**, 534–552 (2020).
4. Wang, X., Pang, G. & Yang, M. Precipitation over the Tibetan Plateau during recent decades: a review based on observations and simulations. *Int. J. Climatol.* **38**, 1116–1131 (2018).
5. Yang, K. et al. Recent climate changes over the Tibetan Plateau and their impacts on energy and water cycle: a review. *Glob. Planet. Change* **112**, 79–91 (2014).
6. Curio, J. & Scherer, D. Seasonality and spatial variability of dynamic precipitation controls on the Tibetan Plateau. *Earth Syst. Dyn.* **7**, 767–782 (2016).
7. Yao, T. et al. A review of climatic controls on δ^{18}O in precipitation over the Tibetan Plateau: Observations and simulations. *Rev. Geophys.* **51**, 111–119 (2013).
8. Jiang, X. et al. Interannual variation of summer atmospheric heat source over the Tibetan Plateau and the role of convection around the western Maritime Continent. *J. Clim.* **29**, 121–138 (2016).
9. Jiang, X. & Ting, M. A dipole pattern of summertime rainfall across the Indian subcontinent and the Tibetan Plateau. *J. Clim.* **30**, 9607–9620 (2017).
10. Jiang, X. & Ting, M. Intraseasonal variability of rainfall and its effect on interannual variability across the Indian subcontinent and the Tibetan Plateau. *J. Clim.* **32**, 2227–2245 (2019).
11. Zhu, Y., Sang, Y., Chen, D., Sivakumar, B. & Li, D. Effects of the South Asian summer monsoon anomaly on interannual variations in precipitation over the South-Central Tibetan Plateau. *Environ. Res. Lett.* **15**, 124067 (2020).
12. Wang, Z., Jiang, X., Ke, Z. & Song, Y. Interannual variation of the onset of the Tibetan Plateau rainy season and its relationship with the sea surface temperature in the North Pacific. *Int. J. Climatol.* **43**, 4662–4676 (2023).
13. Wang, Z., Jiang, X. & Ke, Z. The objective monitoring method of the Tibetan Plateau rainy season and its changing trend over the past 6 decades. (in Chinese). *Chinese J. Geophys.* **66**, 505–517 (2023).
14. Zhang, W., Zhou, T. & Zhang, L. Wetting and greening Tibetan Plateau in early summer in recent decades. *J. Geophys. Res.* **122**, 5808–5822 (2017).
15. Liu, Y. et al. The advanced South Asian monsoon onset accelerates lake expansion over the Tibetan Plateau. *Sci. Bull.* **64**, 1486–1489 (2019).
16. Schiemann, R., Lüthi, D. & Schär, C. Seasonality and interannual variability of the westerly jet in the Tibetan Plateau region. *J. Clim.* **22**, 2940–2957 (2009).
17. Molnar, P., Boos, W. R. & Battisti, D. S. Orographic controls on climate and paleoclimate of Asia: thermal and mechanical roles for the Tibetan Plateau. *Annu. Rev. Earth Planet. Sci.* **38**, 77–102 (2010).
18. Chiang, J. C., Kong, W., Wu, C. H. & Battisti, D. S. Origins of East Asian summer monsoon seasonality. *J. Clim.* **33**, 7945–7965 (2020).
19. Ren, Q., Jiang, X., Zhang, Y., Li, Z. & Yang, S. Effects of suppressed transient eddies by the Tibetan Plateau on the East Asian summer monsoon. *J. Clim.* **34**, 8481–8501 (2021).
20. Xu, X. et al. World water tower: an atmospheric perspective. *Geophys. Res. Lett.* **35**, 525–530 (2008).
21. Sampe, T. & Xie, S. Large-scale dynamics of the meiyu-baiu rainband: Environmental forcing by the westerly jet. *J. Clim.* **23**, 113–134 (2010).
22. Hunt, K. et al. Subtropical westerly jet influence on occurrence of western disturbances and Tibetan Plateau vortices. *Geophys. Res. Lett.* **45**, 8629–8638 (2018).
23. Wang, B. & LinHo. Rainy season of the Asian-Pacific summer monsoon. *J. Clim.* **15**, 386–398 (2002).
24. Zhou, C., Zhao, P. & Chen, J. The interdecadal change of summer water vapor over the Tibetan Plateau and associated mechanisms. *J. Clim.* **32**, 4103–4119 (2019).
25. Wang, Z., Yang, S., Luo, H. & Luo, J. Drying tendency over the southern slope of the Tibetan Plateau in recent decades: role of a CGT-like atmospheric change. *Clim. Dyn.* **59**, 2801–2813 (2022).
26. Chen, B., Zhang, W., Yang, S. & Xu, D. Identifying and contrasting the sources of the water vapor reaching the subregions of the Tibetan Plateau during the wet season. *Clim. Dyn.* **53**, 6891–6907 (2019).

27. Adler, R. F. et al. The version-2 global precipitation climatology project (GPCP) monthly precipitation analysis (1979–present). *J. Hydrometeorol.* **4**, 1147–1167 (2003).
28. Harris, I. et al. Updated high-resolution grids of monthly climatic observations–the CRU TS3. 10 Dataset. *Int. J. Climatol.* **34**, 623–642 (2014).
29. Hersbach, H. et al. The ERA5 global reanalysis. *Q. J. R. Meteorol. Soc.* **146**, 1999–2049 (2020).
30. Hurrell, J. et al. The community earth system model: a framework for collaborative research. *Bull. Am. Meteorol. Soc.* **94**, 1339–1360 (2013).

Acknowledgements

X.J. received financial support from the Second Tibetan Plateau Scientific Expedition and Research program (2019QZKK0106), the National Natural Science Foundation of China (Grants 42075045, U20A2097), the Sichuan Science and Technology Program (Grant 2022YFS0540), and the Youth Innovation Team of China Meteorological Administration "Climate change and its impact in the Tibetan Plateau" (NO. CMA2023QN16). T.Z. received financial support from the National Natural Science Foundation of China (Grants 42175023).

Author contributions

X.J. conceived the idea, performed and calculations, and drafted the manuscript for the study. F.C. downloaded the observational data and performed the calculations. Z.L. performs the model simulations. Z.W. discussed the results throughout the whole process. T.Z. revised the manuscript. All authors discussed the results throughout the whole process, and contributed to the revision.

Competing interests

The authors declare no competing interests.

Additional information

Supplementary information The online version contains supplementary material available at https://doi.org/10.1038/s43247-023-01035-6.

Correspondence and requests for materials should be addressed to Xingwen Jiang.

Peer review information *Communications Earth & Environment* thanks the anonymous reviewers for their contribution to the peer review of this work. Primary Handling Editors: Akintomide Akinsanola and Aliénor Lavergne. A peer review file is available

Reprints and permission information is available at http://www.nature.com/reprints

Publisher's note Springer Nature remains neutral with regard to jurisdictional claims in published maps and institutional affiliations.